Available online at www.CivileJournal.org

Civil Engineering Journal

(E-ISSN: 2476-3055; ISSN: 2676-6957)

Vol. 10, No. 01, January, 2024

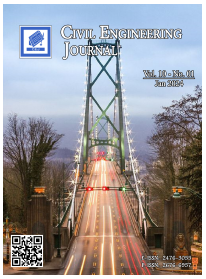

The Application of Neural Networks to Predict the Water Evaporation Percentage and the Plastic Shrinkage Size of Self-Compacting Concrete Structure

Cuong H. Nguyen [1], Linh H. Tran [2*]

[1] *Hanoi University of Civil Engineering, 55 Giai Phong str., Hanoi, Vietnam.*

[2] *Hanoi University of Science and Technology, 1 Dai Co Viet str., Hanoi, Vietnam.*

Received 11 August 2023; Revised 03 December 2023; Accepted 19 December 2023; Published 01 January 2024

Abstract

This article presents a solution using an artificial neural network and a neuro-fuzzy network to predict the rate of water evaporation and the size of the shrinkage of a self-compacting concrete mixture based on the concrete mixture parameters and the environment parameters. The concrete samples were mixed and measured at four different environmental conditions (i.e., humid, dry, hot with high humidity, and hot with low humidity), and two curing styles for the self-compacting concrete were measured. Data were collected for each sample at the time of mixing and pouring and every 60 minutes for the next ten hours to help create prediction models for the required parameters. A total of 528 samples were collected to create the training and testing data sets. The study proposed to use the classic Multi-Layer Perceptron and the modified Takaga-Sugeno-Kang neuro-fuzzy network to estimate the water evaporation rate and the shrinkage size of the concrete sample when using four inputs: the concrete water-to-binder ratio, environment temperature, relative humidity, and the time after pouring the concrete into the mold. Real-field experiments and numerical computations have shown that both of the models are good as parameter predictors, where low errors can be achieved. Both proposed networks achieved for testing results R2 bigger than 0.98, the mean of squared errors for water evaporation percentage was less than 1.43%, and the mean of squared errors for shrinkage sizes was less than 0.105 mm/m. The computation requirements of the two models in testing mode are also low, which can allow their easy use in practical applications.

Keywords: Concrete Dehydration; Plastic Shrinkage; Neuro-Fuzzy Networks; Water Evaporation; Concrete Curing.

1. Introduction

Self-Compacting Concrete (SCC) is a type of concrete with the ability to self-flow and self-compact, filling formwork under its own weight while still ensuring uniformity, even in cases of dense reinforcement [1, 2]. The composition of the concrete mix has some differences compared to ordinary concrete, such as a higher level of fine filler content, a higher superplasticizer admixture, a larger cement paste volume, and a lower W/B (water-to-binder) ratio. Therefore, the behavior of concrete in the early curing stage, specifically water evaporation and plastic shrinkage, will be different from that of conventional concrete, leading to a different curing process. According to Loukili [3], because SCC has a larger fine binder ratio, a low W/B ratio, and a larger dosage of superplasticizers, surface water drainage is usually lower compared with conventional concrete. Simultaneously, cracks due to plastic shrinkage in SCC are more serious than in conventional concrete [4, 5]. The evaporation rate is an essential parameter that directly affects the

* Corresponding author: linh.tranhoai@hust.edu.vn

http://dx.doi.org/10.28991/CEJ-2024-010-01-07

concrete plastic shrinkage, causing long-lasting changes to the strength of concrete structures. Therefore, the estimation of the evaporation rate is important for any fresh concrete prior to entering the pouring process [6]. For SCC, the concrete maintenance will be carried out promptly after pouring concrete to reduce water evaporation from the concrete's surface and reduce the risk of premature cracking.

Controlling the amount of water evaporated in the early curing stage is important to ensure the quality of the concrete. When the rate of water evaporation is too high, the concrete will fall into a state of dehydration, affecting the hydration of cement, leading to a decrease in the bearing strength of the concrete [7]. According to Khoa & Vu [8], when concrete is in the plastic state, the loss of water facilitates the development of plastic shrinkage. If dehydration occurs rapidly, it will cause the plastic shrinkage to quickly reach its maximum and continuously develop in the subsequent stages of concrete (the solid phase). As a result, more cracks will be created in concrete structures [7]. The ACI standard states that precautions should be taken when water evaporation rates reach 1kg/m^2/h. The Australian standard guidelines state that plastic shrinkage cracking occurs when the water evaporation rate reaches a value of 1 kg/m^2/h [9]. For the above reason, there is a need to accurately predict the level of water evaporation and plastic shrinkage in the early curing stage to serve as a basis for effective maintenance of the concrete. Since the parameters of SCC depend nonlinearly on the input components [10, 11], the development of a mathematical model to predict the parameters from the input ingredients and environmental conditions is critical for the calculation of other conditions that were not presented in the learning data samples [12].

To date, there are various studies and resulting models to estimate the parameters of SCC in general and the water evaporation rate (WEP) and concreate shrinkage in particular. Many of these previous research works concentrated on an important factor of the concrete, its compressive strength [13–16]. However, the amount of research concentrating on water evaporation rate and concrete shrinkage is much less. Due to the process complexity, in practice, the evaporation rate assessment is often carried out by site engineers based on the Nomograph developed by ACI [7]. The Nomograph in ACI 305R-10 estimates the rate of evaporation of surface humidity from concrete based on inputs of air temperature, relative humidity, and wind velocity. Alternatively to Nomograph, the work in Khoa and Vu [8] proposed a polynomial function of the three inputs used in Nomograph together with the temperature of the concrete as an additional input. On the other hand, the studies have highlighted that dependencies on the inputs undergo changes when the production technique is altered or new additives are introduced, leading to the need for model updates or re-training with new data.

In Almohammad-albakkar et al. [6], the authors studied the SCC containing micro-silica and/or nano-silica to develop a theoretical drying shrinkage model that could predict both the development trend and final values of drying shrinkage with a mean absolute error (MAE%) at 28 days around 8.62%. Nguyen et al. [10] investigated the development of a predictive model for the plastic shrinkage of SCC (B4TW-SCC) based on 1.216 sets of shrinkage data. The plastic shrinkage was assessed based on input factors, including variations in cement content (with changes up to 40%) and a W/P ratio ranging from 0.36 to 0.48. Meanwhile, Li & Li [11] developed a method for predicting the plastic shrinkage of SCC based on the theory of critical stress and structural voids. With various SCC samples having different compressive strengths prepared, the model's predicted results were found to be in good agreement with the measured values. The impact of different additives on the occurrence and magnitude of plastic shrinkage in SCC was discussed in Turcry & Loukili [12]. The tests were initiated immediately after casting SCC samples, and deformation parameters and pore pressure were monitored. As a result, a mechanism to prevent cracking was identified.

Wang et al. [17] demonstrated that the use of fibers and fly ash to increase the diameter of voids in concrete can reduce tensile forces within the void walls, resulting in reduced plastic shrinkage in concrete. Erten et al. [18] showed that cracks caused by shrinkage can diminish the corrosion resistance of high-performance concrete, and fibers can limit crack formation. Boshoff & Combrinck [19] proposed a model for predicting the shrinkage-induced cracking level based on the W/P ratio during the process from concrete pouring to setting. The model was built based on a large amount of experimental data. Ghoddousu et al. [20] developed an equation to estimate plastic shrinkage values based on the coarse aggregate ratio and W/P ratio under hot-dry climate conditions. The results showed that plastic shrinkage depends on time and has a linear relationship with evaporable water content. In the study of cracking and plastic shrinkage, Qi et al. [21] demonstrated that the higher difference between the water leaving the concrete and the evaporable water from the surface, as well as negative pressure within the voids, leads to an increase in the elastic deformation value of SCC.

However, it can be observed that most of the research primarily focuses on the evaluation of concrete's plastic shrinkage. The estimation of both the plastic shrinkage parameters and the evaporable water content of SCC simultaneously based on changes in the W/P ratio, environmental factors (temperature, humidity), and time remains an unexplored area.

In recent years, in the fields of technology in general and construction technology in particular, artificial neural networks (ANNs) have been studied and applied to model nonlinear relationships between object parameters [22–24] as well as the behavior of materials. According to Haykin [25], the advantage of using ANN is the capability to solve problems that do not have a known or given mathematical model of the object. The object to be forecasted is a function

that depends on many factors or a complex predictor that has a nonlinear relationship with the dependent factors. However, there are not yet any studies using ANN to predict the percentage of water evaporated from the concrete and also the deformation of the concrete structure (measured by the length shrinkage of the samples) in the early stage of curing in Vietnam's climate. Another popular tool recently developed is deep learning networks. They have been successfully used for many signal processing problems, especially for image processing and recognition in construction [26]. However, the main problem with these tools is that a huge set of data samples is required to train them because the number of parameters is much higher compared with the classic models.

In this paper, a new approach to predicting the WEP and the plastic shrinkage size of SCC is proposed. For the purpose of this article, we experimentally mixed 48 base SCC samples to create data sample sets. The computation models predicting the WEP and the plastic shrinkage size of SCC based only on four inputs, including the concrete water-to-binder ratio, environment temperature, relative humidity, and the time after pouring the concrete into the mold. This simple requirement will ease the implementation of the models in practical use. As nonlinear predictors, the classic Multi-Layer Perceptron (MLP) and the modified neuro-fuzzy Takaga-Sugeno-Kang (TSK) network were proposed. These models have been proven highly effective as predictive solutions for various technical problems [10, 13, 14].

2. Method for Determining the Water Evaporation Percentage and the Plastic Shrinkage Size of Samples SCC

The predictive models will receive input from four variables: the W/B ratio of the mixture, the environment temperature and relative humidity, and the time elapsed since pouring the mixture into the mold. The models will also produce four outputs: two rates of the water evaporation percentage (WEP) for samples without and with curing, and two deformation lengths (concrete sample shrinkages) for samples without and with curing. The general methodology of the proposed process is shown in Figure 1.

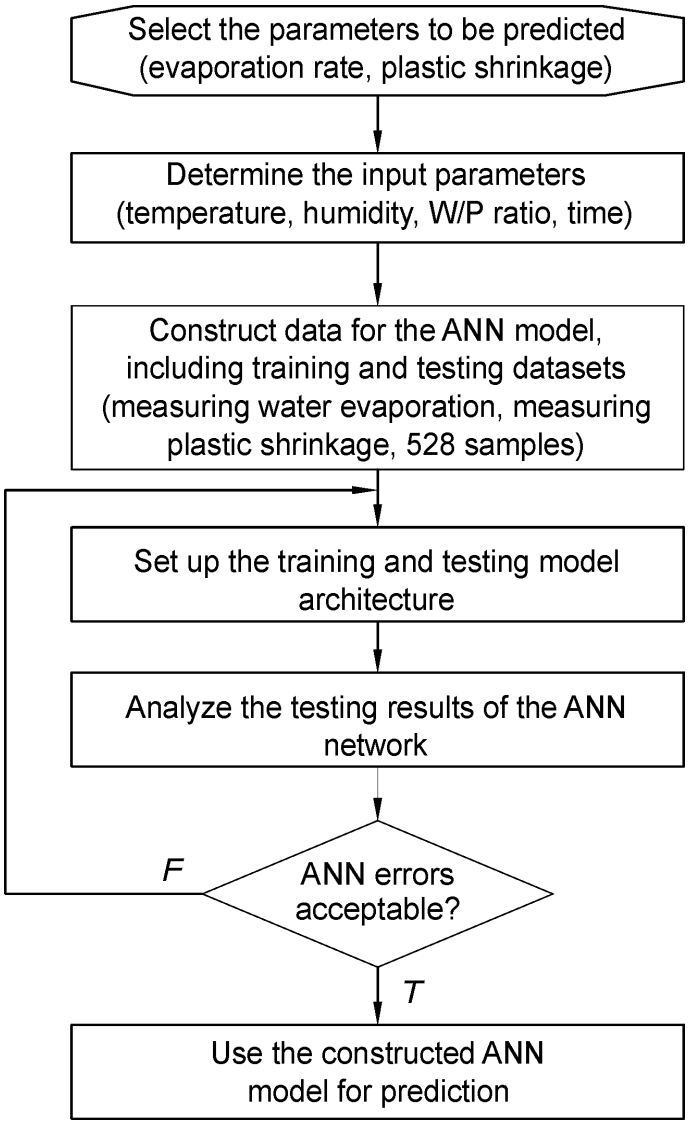

Figure 1. The process of the proposed methodology used for implementing the predictive models

The numerical results showed that both networks can serve effectively as robust nonlinear predictors for WEP and shrinkage size parameters of SCC, with a slight advantage observed in the performance of the modified TSK network.

Water evaporation from concrete is the loss of water to the surrounding environment, influenced by weather factors such as air temperature, air relative humidity, wind speed, and solar radiation. This evaporation process spans several days, with a very high rate in the first 8 to 10 hours after pouring and a much slower rate for the rest of the process [10]. In this study, the volume of water evaporated through the open surface of the SCC was quantified by periodically weighing 10×10×30 cm test specimens on a precision electronic scale with an accuracy of 0.1g (see Figure 2-a). Over a 10-hour period, with the sampling period equal to every one hour, commencing from the time of concrete pouring into the mold, the concrete sample weight was recorded to determine the volume of water evaporated. The concrete samples were tested for water loss in two curing conditions: no curing and water curing.

(a) (b)

Figure 2. Measurement of Plastic Shrinkage of SCC (a) and measuring the water loss of SCC (b)

Plastic shrinkage is a physical process occurring during the initial stages of concrete setting and hardening, primarily driven by the rapid evaporation of water. Water shrinkage increases the negative pressure in the capillaries, causing aggregated particles to come closer together and resulting in deformation within the concrete [10]. In this study, plastic deformation was assessed using two strain gauges positioned at both ends of 10×10×30 cm concrete specimens. Continuous measurements were taken over an 8-hour period (from 10:00 to 18:00), beginning with the initial measurement. The variable value represents the combined output of the two gauges, which was then converted to mm/m based on the combined value of the variable measurement and the length of the specimen. Concrete samples were subjected to testing under two distinct curing conditions, including no curing and water curing (see Figure 2-b).

The experiment was conducted in the natural environmental conditions of the Hanoi region of Vietnam. Four distinct weather conditions (namely C_1, C_2, C_3, and C_4) were selected based on their relative suitability with the typical weather regions of Vietnam's hot and humid climate, including different climate seasons and parameters. The experiment conditions are shown in Table 1.

Table 1. Weather conditions used in generating samples

Symbol	Characteristics	Air temperature (ºC)	Air humidity (%)
C1	Wet, hot	15 to 30	70 to 95
C2	Dry	18 to 30	40 to 65
C3	Hot, humid	28 to 35	65 to 85
C4	Hot	28 to 40	40 to 65

The measurements of evaporation served to calculate the cumulative percentage of water evaporated from the sample at each measurement interval, relative to the total quantity of water used during the concrete sample's mixing process.

Table 2 shows two illustrative sets of measurement results obtained at different temperature and relative humidity (RH%) conditions, as well as two distinct curing conditions.

Table 2. Examples of Water Evaporation Percentage and Shrinkage size measurement

Time (h)	T (ºC)	RH (%)	WEP (%)		Plastic shrinkage size (mm/m)	
			without curing	with curing	without curing	with curing
Sample No. 1						
0	26	50	0	0	0	0
1	30	40	3.39	3.1	0	0
2	32	41	7.28	6.1	0	0
3	32	40	16.94	13.97	-1.22	-0.91
4	32	45	22.36	19.1	-1.83	-1.51
5	31	42	27.1	23.2	-2.1	-1.81
6	31	50	30.91	26.5	-2.31	-2.07
7	28	52	32.58	28.2	-2.35	-2.1
8	28	55	32.58	28.2	-2.43	-2.13
9	27	60	32.58	28.2	-2.43	-2.13
10	26	63	32.58	28.2	-2.43	-2.13
Sample No. 2						
0	30	85	0	0	0	0
1	31	75	3.7	3.4	0	0
2	35	65	8.9	8.1	0	0
3	33	67	12.3	11.4	-0.74	-0.59
4	32	68	15.1	14.1	-1.11	-0.89
5	32	68	17.5	16.4	-1.35	-1.08
6	31	69	19.57	18.1	-1.45	-1.17
7	30	70	20.7	18.85	-1.47	-1.19
8	29	72	20.91	18.9	-1.5	-1.21
9	28	75	20.91	18.9	-1.5	-1.21
10	28	76	20.91	18.9	-1.5	-1.21

3. The Neural Network and Neuro-Fuzzy Network as Nonlinear Estimators

The prediction models are represented by nonlinear transfer functions between input vectors and output vectors. Typically, as in this research, when the transfer function is not known in advance, the model's parameters are determined based on machine learning algorithms and some data sample sets. In the classic approach of the supervised mode of training, there are at least two data sets required: the learning data set and the testing data set [25].

If we denoted the learning data samples set containing p pairs of input-output $\{x_i, d_i\}$ where $i = 1,\dots,p$; $x_i \in \mathbb{R}^N$; $d_i \in \mathbb{R}^K$ then the parameters w of a function $f()$ are adapted during the learning process to minimize the error function, also called the sum squared error (SSE) function:

$$E_{learn} = \frac{1}{2}\sum_{i=1}^{p}\|f_w(\boldsymbol{x}_i) - \boldsymbol{d}_i\|^2 \rightarrow min \quad (1)$$

When the learning process ends, the achieved function is tested with new set of q pairs of data $\{x_i^{test}, d_i^{test}\}$ where $i = 1,\dots,q$. The different measures to evaluate the performance, among which we can use again SSE function:

$$E_{test} = \frac{1}{2}\sum_{i=1}^{p}\|f_w(\boldsymbol{x}_i^{test}) - \boldsymbol{d}_i^{test}\|^2 \quad (2)$$

or other measures such as the mean relative error (MRE), the correlation score, etc. [25].

Throughout the testing process, the parameters of the function (indicated as components in w) remain unaltered. When multiple model candidates were available, the one with the lowest testing error was chosen as the optimal choice. As previously mentioned, in this research, we will use MLP and modified TSK models to assess their performance with the data sets we collected.

3.1. The Multi-Layer Perceptron

The MLP is a feedforward structure with one input layer, one output layer, and some hidden layers [25]. There is no limitation on the number of hidden layers, but the most popular configuration is the MLP with one hidden layer.

In Figure 3, an example of MLP network with 1 hidden layer is presented with *N* inputs, *M* neurons in the hidden layer and *K* outputs. It's also recommended that each neuron should have a so-called bias input equal 1. The connections from the inputs to the hidden neurons are denoted by the weights W_{ij} $(i = 1, \dots, M; j = 0, \dots N)$ the connections from the hidden neurons to the outputs are denoted by V_{ij} $(i = 1, \dots, K; j = 0, \dots, M)$.

The transfer function of hidden neurons is denoted as f_1, and the transfer function of output neurons is f_2. The popular selection of f_1 is the $tansig()$ defined as follow [22]:

$$f_1(x) = tansig(x) = \frac{e^x - e^{-x}}{e^x + e^{-x}} \quad (3)$$

and linear function for f_2 [22].

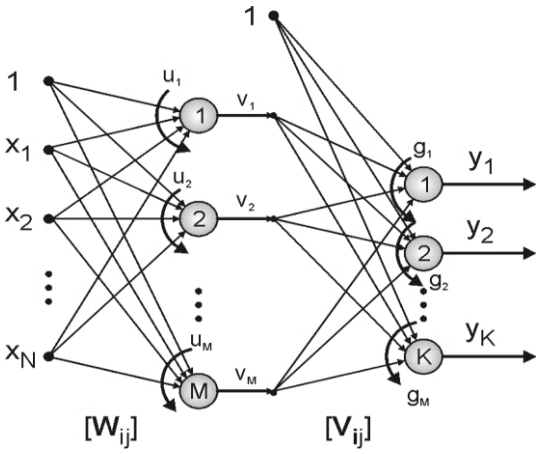

Figure 3. An example of MLP with one hidden layer

With the above descriptions, the output of the MLP is calculated as a feedforward network for an input vector $\boldsymbol{x} = [x_1, x_2, \dots, x_N] \in \mathbb{R}^N$ as follow:

1. The aggregated inputs of hidden neurons:

$$u_i = \sum_{j=0}^{N} W_{ij} \cdot x_j \quad (4)$$

2. Outputs of hidden neurons v_i for $i = 1, \dots, M$ (let $v_0 = 1$):

$$v_i = f_1\left(\sum_{j=0}^{N} W_{ij} \cdot x_j\right) \quad (5)$$

3. Outputs of the MLP network y_k for $k = 1, \dots, K$:

$$y_k = f_2\left(\sum_{i=0}^{M} V_{ki} \cdot v_i\right) \quad (6)$$

or in a simplified form as:

$$y_k = f_2\left(\sum_{i=0}^{M} \left[V_{ki} \cdot f_1\left(\sum_{j=0}^{N} W_{ij} x_j\right)\right]\right) \quad (7)$$

When the data sample sets are provided, the number of inputs and the number of outputs of an MLP align with the corresponding dimensions of the input and output vectors in the sample sets. However, the appropriate number of hidden neurons is not straightforward and needs to be determined.

For a given number of hidden neurons, the MLP undergoes training to fit a designated set of learning data samples, involving the adjustment of weights W_{ij} and V_{ij}. In this paper, the classic Levenberg–Marquadrt algorithm was used to train the MLPs [25]. The selection of the optimal number of hidden neurons was determined using a trial-and-error approach, similar to the method outlined in Nguyen & Tran [22] and Haykin [25].

3.2. The modified TSK Neuro-fuzzy Network

The second nonlinear estimator that is used for testing in this paper is a modified version of the neuro-fuzzy TSK network, whose structure is presented in Figure 4, where *N* indicates the number of inputs and *M* denotes the number of reasoning rules. For the sake of clarity, the network in Figure 3 shows only one output, although it's important to note that this model can be configured for any desired number of outputs. This modified model has two significant deviations from the original TSK model [27]:

- It uses the Mahalanobis distance instead of the Euclidean distance in the membership function, and
- It abstains from computing the averages of weights in the final response.

For an input vector $x = [x_1, x_2, \dots, x_N] \in \mathbb{R}^N$, in the classic TSK network, the output membership value indicating "how close vector x is to a center point $c_i = [c_{i1}, c_{i2}, \dots, c_{iN}]$" is as follow:

$$\mu_i(\boldsymbol{x}) = \prod_{j=1}^{N} \mu_i(x_j) = \prod_{j=1}^{N} \frac{1}{1+\left(\frac{x_j - c_{ij}}{\sigma_{ij}}\right)^{2b_{ij}}} \tag{8}$$

where it can be clearly seen the use of Euclidean distances between each dimension of x and c_i. Therefore, the number of so-called width parameters σ_{ij} is $N \times M$ and the number of so-called shape parameters b_{ij} is also $N \times M$.

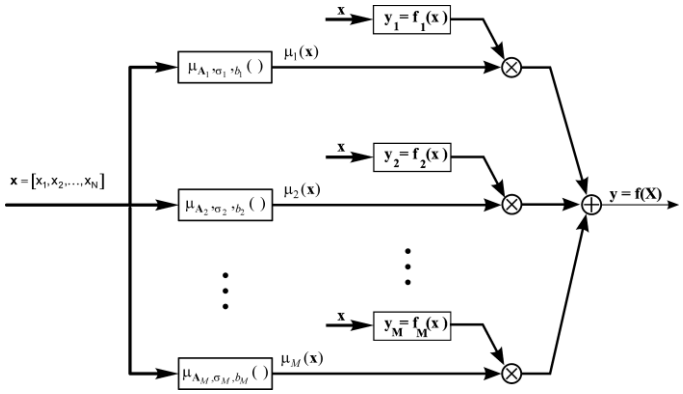

Figure 4. An example of a modified TSK network with one output

In the modified network, the Mahalanobis measure is used as the distance between **x** and $\mathbf{c}_i$ with the formula:

$$\|x - c_i\|_M = \sqrt{\|x - c_i\|^T \cdot A_i \cdot \|x - c_i\|} \tag{9}$$

where A_i is the so-called scaling matrices. It can be seen that the Euclidean distance is a special case of the Mahalanobis distance, where the scaling matrices are identity matrices.

With this measure, the membership function is determined as follow:

$$\mu_i(\boldsymbol{x}) = \frac{1}{1+\left(\frac{\|x - c_i\|_M}{\sigma_i}\right)^{2b_i}} \tag{10}$$

The introduction of scaling matrix A_i for each reasoning rule initially serves to reduce the number of width parameters σ_i to M only (one parameter for one rule) and the shape parameter b_i also to M only. On the other hand, the scaling matrices allow a better penetration of the rules into the space of features, which, in turn, would facilitate improved data modelling. A demonstration of this enhanced data space penetration and representation is shown on Fig. 5, where data samples are grouped into three areas. As depicted in Figure 5-a, that different scales in data dimensions have no influence on the Euclidean distance, therefore the equi-distance lines have circular shapes. In contrast, the Mahalanobis distance, by taking into account the correlations of the data points, leads to equidistant lines having the rotated elliptical shapes, as illustrated in Figure 5-b. These shapes, in turn, would generate a better data representation for further computation blocks in our proposed model.

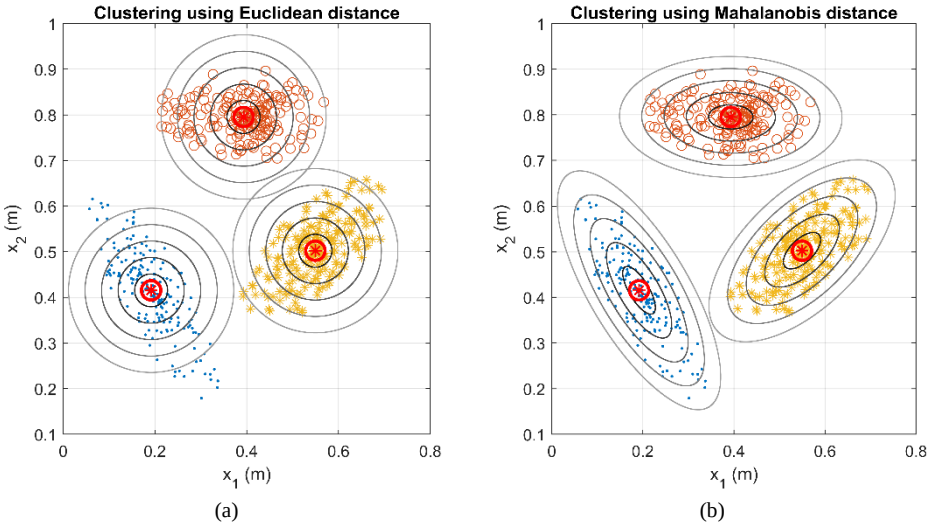

Figure 5. (a) A demonstration of clustering of 2-D data samples using Euclidean distance, (b) and using Mahalanobis distance

The modified TSK network uses the same linear TSK function $f_i(x)$, for $i = 1, \dots, M$, as in the classic network, with the outputs are:

$$f_i(x) = q_{i0} + \sum_{j=1}^{N} q_{ij} x_j \quad (11)$$

where q_{ij} are linear parameters to be trained.

For the classic network, the final output is a *weighted* response from all the reasoning rules:

$$y = \frac{\sum_{i=1}^{M} \mu_i(x) \cdot f_i(x)}{\sum_{i=1}^{M} \mu_i(x)} \quad (12)$$

but the modified TSK uses just the numerator of Equation 12, i.e. the output of the modified TSK is as follow:

$$y = \sum_{i=1}^{M} \mu_i(x) \cdot f_i(x) \quad (13)$$

This simplification has a significant impact on the training algorithm of the network [27]. In the classical approach, the denominator also includes trainable parameters, resulting in complex gradient formulas and requiring more computational operations. However, despite the introduction of the matrix A_i, it does not significantly complicate the learning process, as it was shown in Linh [27] that the matrices can be determined once after the initialization of the data centers using fuzzy clustering method and they don't need to be updated during the training of other parameters. For a data set containing p input samples x_j and M data centers c_i, the determination of matrix A_i is as follow:

- Calculate the degrees u_{ji} (also called the membership values) that a sample vector x_j belong to a centers c_i (for $j = 1,2, \dots, p;\ i = 1,2, \dots, M$):

$$u_{ji} = \frac{\frac{1}{\|x_i - c_j\|^2}}{\sum_{k=1}^{M} \frac{1}{\|x_i - c_k\|^2}} \quad (14)$$

- Calculate the matrices of covariation F_i for $i = 1,2, \dots, M$:

$$F_i = \sum_{j=1}^{p} u_{ji}^2 (x_j - c_i) \cdot (x_j - c_i)^T \quad (15)$$

- Calculate the scaling matrices A_i for $i = 1,2, \dots, M$:

$$A_i = \sqrt[N]{det(F_i)} \cdot F_i^{-1} \quad (16)$$

In the case of the TSK network, similar to the MLP network, the number of inputs and outputs is determined by the data samples. During the training process, it's needed to find the number of rules that enable the network to achieve a desirable low level of testing errors. We used a similar "trial and test" approach, starting with a network containing just one rule and increasing the number of rules during these trials [22]. To train the TSK networks, the hybrid algorithm described in Linh [27] was used.

4. Field Experiments and Numerical Results

In this section, the experiments to mix the concrete samples and measure the evaporation rates at different time points will be discussed. With the collected data samples, the two networks are trained with different networks' structures to experimentally determine the best candidates for the prediction tasks discussed in Section 1 and Section 2.

4.1. Sample Mixtures Preparation and Data Collections

In order to create the data samples, we mixed a total of 48 samples of SCC, with 7 main components [28]:

- Cement: from 17.3 to 18.8%;
- Fly ash: from 5.9 to 6.2%;
- Sand: around 34.2%;
- Stone: around 32.6%;
- Super ductile additive: from 0.23 to 0.25%;
- Viscosity modifying admixtures: 0.008% to 0.0085%;
- Water: from 7.8 to 8.3%.

These mixtures allow for a W/B ratio within the range of 0.3 to 0.35. Each mixture was then poured into two molds, one for testing with curing and the other without curing. Each test spanned a duration of 10 hours, measuring the water evaporation and the concrete shrinkage at every hour. Each measurement generates a row of data, as shown in Table 2. Then, for each mixture, half of the samples were used for measuring 11 points without curing, while the remaining half was used for measuring 11 points of samples with curing. As total, $11 \times 48 = 528$ samples were collected. With these 48 sets, we randomly selected 32 sets (i.e., 2/3 of the total) containing 352 samples to form the learning set and the rest of the 176 samples to form the testing set.

The collected WEP and shrinkage sizes are illustrated in Figure 6. It can be evidently seen that when the concrete samples are cured with water surfacing, both the corresponding WEP and shrinkage are reduced as expected.

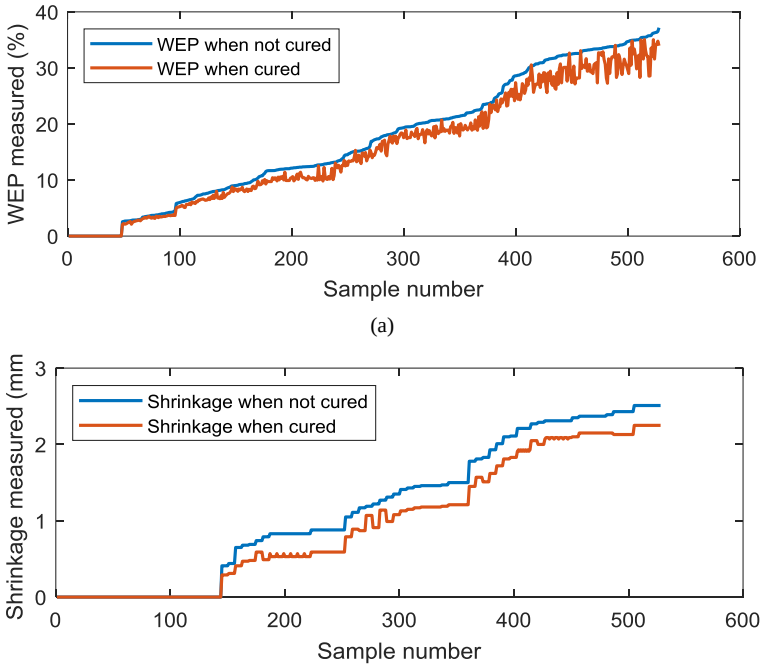

Figure 6. The measured of WEP (a), and shrinkage (b) for the SCC samples mixed in the experiments for cases without curing (blue) and with curing (red)

With those collected data samples, the next task is to train the network models. As previously mentioned, the networks' structure parameters, i.e., the number of hidden neurons in the MLP network and the number of reasoning rules in the TSK network, were selected based on the method of "trial and error". To identify sub-optimal values for these parameters, we randomly generated multiple networks with varying configurations, then trained and tested them with the data sets generated above. The network with the lowest test error was selected for further consideration.

In this study, we used the Mean of Squared Errors (MSE) and Square of Correlation Coefficients (R^2) between the expected values and the actual outputs to compare the performance of the models. In Figure 7, the changes in testing MSE error of MLP networks and TSK networks versus the number of hidden neurons are presented. As can be seen in Figure 7-a for the MLP network, when the number of hidden neurons is greater than 30, practically the testing error stays at a similar level, and the network with 39 hidden neurons achieved the lowest testing error. Consequently, this network was selected for further consideration.

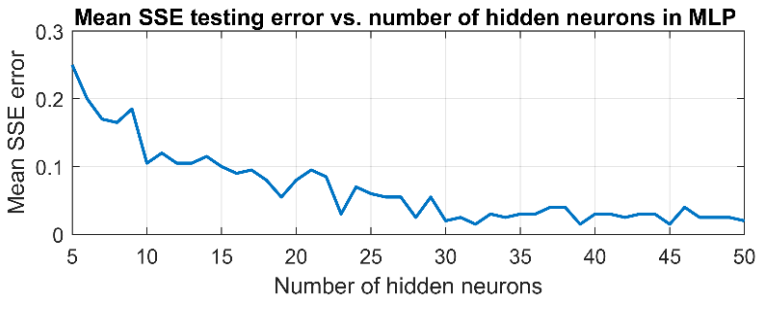

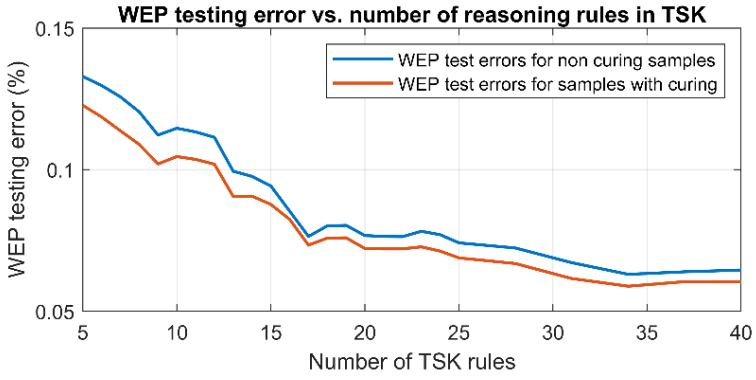

(b)

Figure 7. The changes in testing error versus structure parameter for MLP (a), and TSK (b) networks

A similar result was achieved for the modified TSK network, as depicted in Figure 7-b. The testing errors stabilized after 30, and the network with 34 reasoning rules obtained the lowest testing error. With that, the TSK network with 34 reasoning rules was selected for further consideration.

4.2. Numerical Results

As seen in Figure 7-a, after testing many MLP networks with different numbers of hidden neurons, the MLP network with 39 hidden neurons was selected as the configuration that delivered the best performance. As mentioned earlier, the network has four parallel outputs to estimate the following: 1. WEP for non-cured concrete; 2. WEP for concrete cured with water; 3. shrinkage size for non-cured concrete samples; and 4. shrinkage size for concrete samples cured with water. The testing results (conducted on the set of 176 samples after learning with the other 352 samples) for WEP are presented in Figure 8. The MSE error for no-cured samples was 1.428%, and for samples with curing, it was 1.343%. The corresponding R^2 were 0.9843 and 0.9835.

The results for the prediction of shrinkage sizes for both cases (samples without and with curing) using MLP are shown in Figure 9. The MSE error for no-cured samples was 0.0974 mm/m and for samples with curing it was 0.101 mm/m, where the corresponding R^2 were 0.9886 and 0.9851.

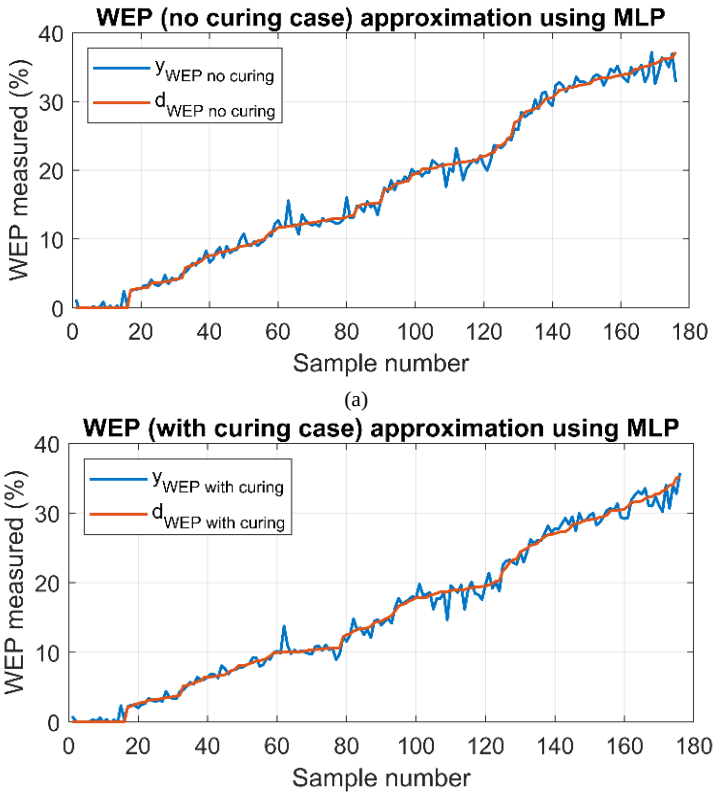

(a)

(b)

Figure 8. The testing error of MLP network for water evaporation percentage prediction for concrete samples (a) without curing, and (b) with curing

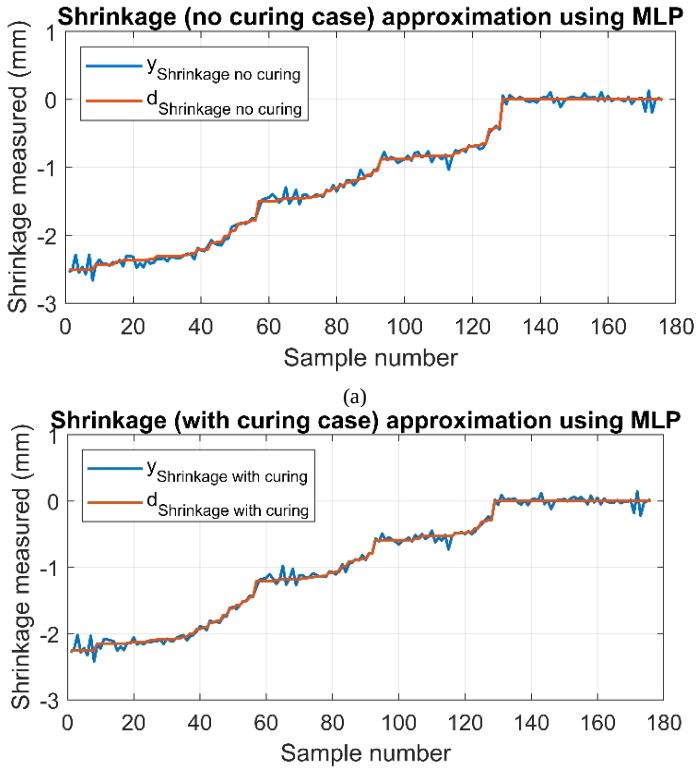

Figure 9. The testing error of MLP network for deformation (in mm) of concrete samples (a) without curing and (b) with curing

The results for WEP and shrinkage estimations were very satisfactory for us; the errors were at very low levels, which shows the great capability of the MLP network to learn nonlinear problems. With a similar process, the TSK models were trained on the same data sets. As seen in Figure 7-b, after testing many TSK networks with different numbers of reasoning rules, the TSK network with 34 reasoning rules was selected as the best configuration. The networks were trained to generate similar 4 outputs in parallel as the MLP network. The testing results for WEP are shown in Figure 10. For the TSK network, the MSE error for no cured samples was 1.009%, and for samples with curing, it was 1.014%. The corresponding R^2 were 0.9922 and 0.9906, respectively.

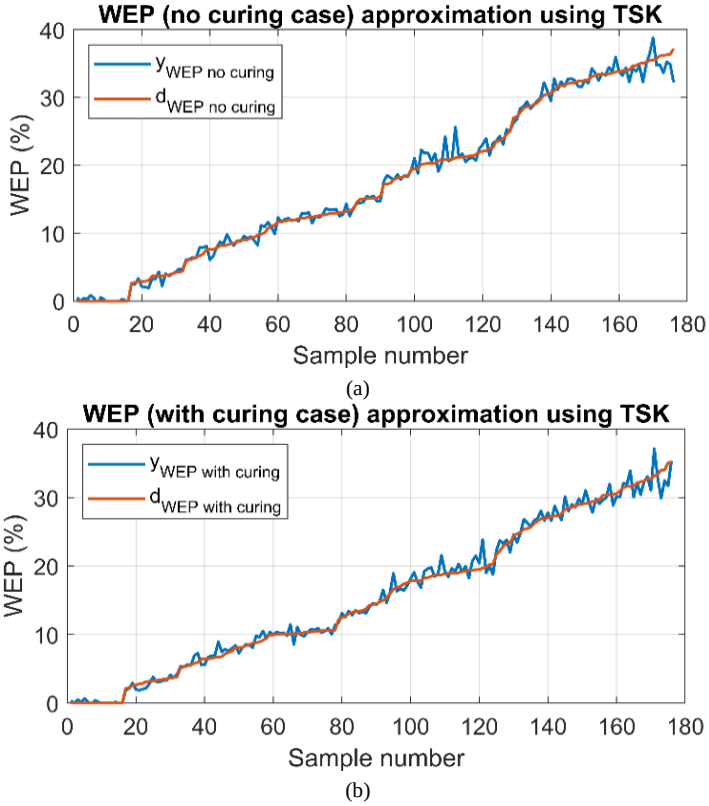

Figure 10. The testing error of TSK network for water evaporation percentage prediction for concrete samples (a) without curing and (b) with curing

The results for using TSK to predict the shrinkage sizes for both cases (samples without and with curing) are shown in Figure 11. The MSE error for no cured samples was 0.0778 mm/m and for samples with curing it was 0.0768 mm/m, where the corresponding R^2 were 0.9926 and 0.9910. The results for WEP and shrinkage estimations were again very satisfactory, relatively even better than the performance of the MLP.

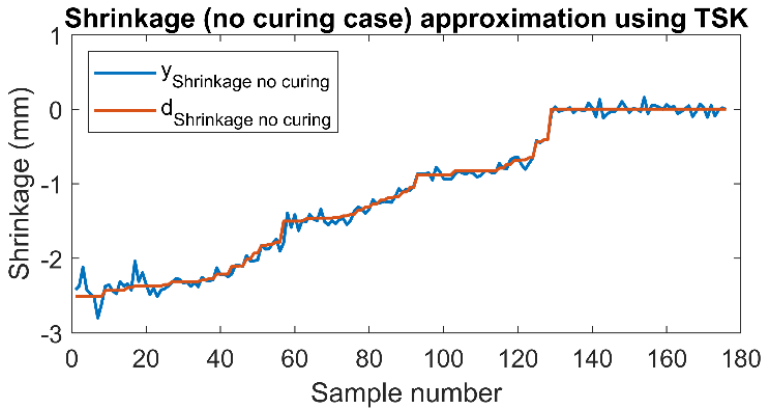

(a)

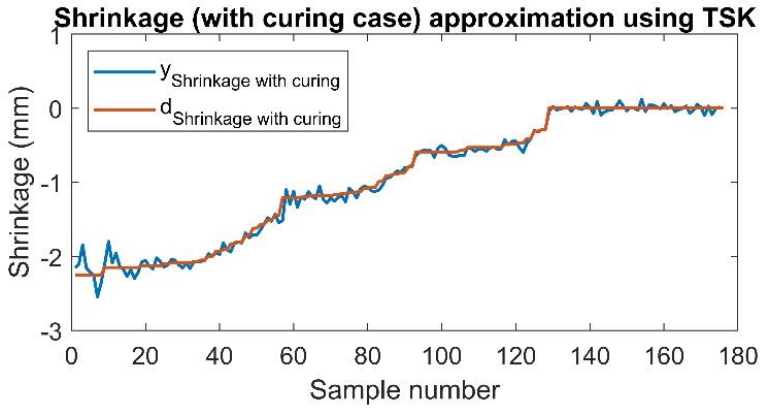

(b)

Figure 11. The testing error of TSK network for deformation (in mm) of concrete samples (a) without curing and (b) with curing

The results for both cases are collected in Tables 3 and 4 for comparison purposes.

Table 3. Mean squared error for testing samples

Case	MLP (39 hidden neurons)	TSK (34 reasoning rules)
WEP no curing (%)	1.428	1.009
WEP with curing (%)	1.343	1.014
Shrinkage when no curing (mm/m)	0.0974	0.0778
Shrinkage when with curing (mm/m)	0.101	0.0768

Table 4. R^2 coefficient for testing samples

Case	MLP (39 hidden neurons)	TSK (34 reasoning rules)
WEP no curing	0.9843	0.9922
WEP with curing	0.9835	0.9906
Shrinkage when no curing	0.9886	0.9926
Shrinkage when with curing	0.9851	0.9910

5. Conclusion

The paper presented the application of MLP and the modified TSK networks to estimate the water evaporation rates and the shrinkage size of SCC samples for different environmental conditions. The SCC samples were tested when not cured and when curing with water. Experimental specimens of concrete were mixed and measured to create a total of 528 data samples for training and testing the networks. Numerical results showed that both networks can be trained from the data sets to make highly accurate predictions of WEP and shrinkage size for both cured and not cured concrete samples. Comparatively, the TSK network showed better performance than MLP for the data sets used. The networks required only four inputs, including the concrete water-to-binder ratio, environment temperature, relative humidity, and the time after pouring the concrete into the mold. These inputs are straightforward to implement, making the proposed solutions readily adaptable for practical uses.

Based on the achieved results, there are various opportunities to expand the proposed solutions. First, the effectiveness of the models can be significantly enhanced by using additional input parameters such as solar radiation, wind speed, or the actual temperature of the concrete sample. These environmental factors are known to have an impact on the concrete's workability and parameters. Another important factor in the behavior of the SCC is the concrete curing methods. Once the models are trained to predict the SCC's parameters based on curing methods, we can use the results to select the method that gets the best performance from the SCC. Inversely, we are also going to use the data samples for inverse parameter search, where users can estimate the inputs, i.e., the parameters of the concrete or the parameters of the environment, in order to achieve the expected WEP or shrinkage sizes of the mixed SCC samples.

6. Declarations

6.1. Author Contributions

Conceptualization, C.H.N. and L.H.T.; methodology, C.H.N. and L.H.T.; software, L.H.T.; validation, C.H.N. and L.H.T.; formal analysis, C.H.N. and L.H.T.; investigation, C.H.N. and L.H.T.; resources, C.H.N. and L.H.T.; writing—original draft preparation, C.H.N.; writing—review and editing, L.H.T.; visualization, L.H.T.; supervision, C.H.N. and L.H.T.; project administration, C.H.N. All authors have read and agreed to the published version of the manuscript

6.2. Data Availability Statement

The data presented in this study are available on request from the corresponding author.

6.3. Funding

The authors received no financial support for the research, authorship, and/or publication of this article.

6.4. Conflicts of Interest

The authors declare no conflict of interest.

7. References

[1] Ahmad, S., & Umar, A. (2018). Rheological and mechanical properties of self-compacting concrete with glass and polyvinyl alcohol fibres. Journal of Building Engineering, 17, 65–74. doi:10.1016/j.jobe.2018.02.002.

[2] Ahmad, S., Umar, A., Masood, A., & Nayeem, M. (2019). Performance of self-compacting concrete at room and after elevated temperature incorporating Silica fume. Advances in Concrete Construction, 7(1), 31–37. doi:10.12989/acc.2019.7.1.031.

[3] Loukili, A. (2013). Self-compacting concrete. John Wiley & Sons, Hoboken, United States.

[4] Sayahi, F., Emborg, M., & Hedlund, H. (2017). Effect of water-cement ratio on plastic shrinkage cracking in self-compacting concrete. 23th Symposium on Nordic Concrete Research & Development, 21-23 August, 2017, Aalborg, Denmark.

[5] Alaj, A., Krelani, V., & Numao, T. (2023). Effect of Class F Fly Ash on Strength Properties of Concrete. Civil Engineering Journal (Iran), 9(9), 2249–2258. doi:10.28991/CEJ-2023-09-09-011.

[6] Almohammad-albakkar, M., Behfarnia, K., & Mousavi, H. (2022). Estimation of drying shrinkage in self-compacting concrete containing micro- and nano-silica using appropriate models. Innovative Infrastructure Solutions, 7(5), 324. doi:10.1007/s41062-022-00914-9.

[7] Khoa, H. N., & Cường, N. H. (2011). Specification of effective methods to well-maintain concrete in hot-and-humid climate. Journal of Construction Science and Technology (KHCNXD) - University of Social Sciences and Humanities, 5(1), 33-39. (In Vietnamese).

[8] Khoa, H. N., Vu, N. T. (2015). Curing monolithic concrete by membrane in the climate condition of Quang Nam - Da Nang region. Journal of Structural Engineering and Construction Technology, 17, 30–42.

[9] Uno, P. J. (1998). Plastic shrinkage cracking and evaporation formulas. ACI Materials Journal, 95(4), 365–375. doi:10.14359/379.

[10] Nguyen, D.-B., Wu, C.-J., & Liao, W.-C. (2023). Shrinkage Behavior and Prediction Model of Self-Compacting Concrete. Journal of Materials in Civil Engineering, 35(12), 4023454. doi:10.1061/jmcee7.mteng-15808.

[11] Li, Y., & Li, J. (2014). Capillary tension theory for prediction of early autogenous shrinkage of self-consolidating concrete. Construction and Building Materials, 53, 511–516. doi:10.1016/j.conbuildmat.2013.12.010.

[12] Turcry, P., & Loukili., A. (2006). Evaluation of Plastic Shrinkage Cracking of Self-Consolidating Concrete. ACI Materials Journal, 103(4), 272-280. doi:10.14359/16611.

[13] Onyelowe, K. C., Gnananandarao, T., Ebid, A. M., Mahdi, H. A., Razzaghian Ghadikolaee, M., & Al-Ajamee, M. (2022). Evaluating the Compressive Strength of Recycled Aggregate Concrete Using Novel Artificial Neural Network. Civil Engineering Journal (Iran), 8(8), 1679–1693. doi:10.28991/CEJ-2022-08-08-011.

[14] Vakhshouri, B., & Nejadi, S. (2018). Prediction of compressive strength of self-compacting concrete by ANFIS models. Neurocomputing, 280, 13-22. doi:10.1016/j.neucom.2017.09.099.

[15] Faraj, R. H., Mohammed, A. A., Mohammed, A., Omer, K. M., & Ahmed, H. U. (2022). Systematic multiscale models to predict the compressive strength of self-compacting concretes modified with nanosilica at different curing ages. Engineering with Computers, 38(3), 2365–2388. doi:10.1007/s00366-021-01385-9.

[16] Chang, W., & Zheng, W. (2022). Compressive strength evaluation of concrete confined with spiral stirrups by using adaptive neuro-fuzzy inference system (ANFIS). Soft Computing, 26(21), 11873–11889. doi:10.1007/s00500-022-07001-2.

[17] Wang, K., Shah, S. P., & Phuaksuk, P. (2002). Plastic Shrinkage Cracking in Concrete Materials—Influence of Fly Ash and Fibers. ACI Materials Journal, 98(6). doi:10.14359/10846.

[18] Erten, E., Yalçınkaya, Ç., Beglarigale, A., Yiğiter, H., & Yazıcı, H. (2017). Effect of early age shrinkage cracks on corrosion of embedded reinforcement in ultra-high performance concrete with/without fibres. Journal of Gazi University Faculty of Engineering and Architecture, 32(4), 1347–1364. doi:10.17341/gazimmfd.369857. (In Turkish).

[19] Boshoff, W. P., & Combrinck, R. (2013). Modelling the severity of plastic shrinkage cracking in concrete. Cement and Concrete Research, 48, 34–39. doi:10.1016/j.cemconres.2013.02.003.

[20] Ghoddousi, P., Abbasi, A. M., Shahrokhinasab, E., & Abedin, M. (2019). Prediction of Plastic Shrinkage Cracking of Self-Compacting Concrete. Advances in Civil Engineering, 2019, 1–7. doi:10.1155/2019/1296248.

[21] Qi, C., Weiss, J., & Olek, J. (2003). Characterization of plastic shrinkage cracking in fiber reinforced concrete using image analysis and a modified Weibull function. Materials and Structures, 36(6), 386–395. doi:10.1007/bf02481064.

[22] Nguyen, C. H., & Tran, L. H. (2023). Applications of Neural Network and Neuro-Fuzzy Network to Estimate the Parameters of Self-Compacting Concrete. International Journal of GEOMATE, 24(106), 120–129. doi:10.21660/2023.106.3656.

[23] Zhang, X., Dai, C., Li, W., & Chen, Y. (2023). Prediction of compressive strength of recycled aggregate concrete using machine learning and Bayesian optimization methods. Frontiers in Earth Science, 11. doi:10.3389/feart.2023.1112105.

[24] Thirumalai Raja, K., Jayanthi, N., Leta Tesfaye, J., Nagaprasad, N., Krishnaraj, R., & Kaushik, V. S. (2022). Using an Artificial Neural Network to Validate and Predict the Physical Properties of Self-Compacting Concrete. Advances in Materials Science and Engineering, 2022, 1–10. doi:10.1155/2022/1206512.

[25] Haykin, S. (2009). Neural Networks and Learning Machines (3rd Ed.). Pearson Education India, Bengaluru, India.

[26] Ojeda, J. M. P., Cayatopa-Calderón, B. A., Huatangari, L. Q., Tineo, J. L. P., Pino, M. E. M., & Pintado, W. R. (2023). Convolutional Neural Network for Predicting Failure Type in Concrete Cylinders During Compression Testing. Civil Engineering Journal (Iran), 9(9), 2105–2119. doi:10.28991/CEJ-2023-09-09-01.

[27] Linh, T. H. (2002). The modification of TSK network in neuro-fuzzy systems. XXV SPETO, Ustron, 525-528.

[28] el Asri, Y., Benaicha, M., Zaher, M., & Hafidi Alaoui, A. (2022). Prediction of the compressive strength of self-compacting concrete using artificial neural networks based on rheological parameters. Structural Concrete, 23(6), 3864–3876. doi:10.1002/suco.202100796.